Martinez-Roman, J.; Puche-Panadero, R.; Sapena-Bano, A.; Burriel-Valencia, J.; Terrón-Santiago, C.; Pineda-Sanchez, M.; Riera-Guasp, M. (2022). Fast Numerical Model of Power Busbar Conductors Through the FFT and the Convolution Theorem. IEEE Transactions on Power Delivery. 37(4):1-11. https://doi.org/10.1109/TPWRD.2021.3126265

Fast Numerical Model of Power Busbar Conductors Through the FFT and the Convolution Theorem

Javier Martinez-Roman, Ruben Puche-Panadero, *Member, IEEE,*, Angel Sapena-Bano, Jordi Burriel-Valencia, Carla Terron-Santiago, Manuel Pineda-Sanchez, *Member, IEEE*, Martin Riera-Guasp, *Senior Member, IEEE*

***Abstract*—Skin and proximity effects can cause a non-uniform current distribution in the electrical conductors used in alternating current (ac) busbar systems, which increases resistance, decreases internal inductance, and causes asymmetries in the electromagnetic fields and forces. As no explicit solution for the ac resistance or the ac internal inductance of a rectangular conductor has been found, numerical methods are needed to obtain the distribution of the currents inside the busbars. In this paper, a novel numerical approach, based on the fast Fourier transform (FFT) and the convolution theorem, is proposed to model the rectangular conductors of the busbar system, based on the subdivision of the conductor in filamentary subconductors. This technique is know to lead to a dense, huge inductance matrix, that must be multiplied by the current vector, which limits its practical application. The proposed method replaces this matrix-vector multiplication with a simple element-wise vector product in the spatial frequency domain. The FFT speed makes the proposed method very fast and easy to apply. This approach is theoretically explained and applied to an industrial busbar system.**

***Index Terms*—Current density, inductance, skin effect, spectral analysis, convolution.**

I. Introduction

THE dc resistance and the internal inductance of the conductors used in ac power transmission and distribution lines depends on the resistivity of their component wires, their temperature, and their geometry [1]. But, with ac, the current also causes the skin effect within the conductors. Besides, the currents flowing in other conductors that run closely parallel also cause proximity effects. Both effects increase the resistance and reduce the internal inductance of the conductor, giving raise to an increased power loss, which depends on the current frequency. Another consequence of these aggregated effects is that the distribution of the current density within the conductor is not uniform [1]. The change of the electrical parameters of the conductors with the frequency has a direct impact in the design of grounding and bonding systems [2], in the resonance analysis of long transmission cables in offshore wind farms [3], in the shielding of electric automotive power trains cables [4], in the calculation of rail impedances in traction power systems [5], in the analysis of over-voltages in motors connected to frequency converters through long cables [6], in the design of the windings of high speed electrical machines [7], in electromagnetic compatibility analysis [8], or in the computation of eddy loses in Litz wires [9], among many other technological applications.

A particular type of distribution lines widely employed for electrical energy distribution are modular busbar systems [10], because they are fast and easy to install, modify and maintain [11]. As [10] states, high-current busbars with rectangular cross-section are often used in power substations and switching stations, with rated currents up to 10 kA and rated voltages in the range of 10-30 kV. Busbar systems consist of massive copper or aluminum rectangular conductors, which are subject to skin and proximity effects at the industrial frequency. The current density inside this type of massive conductors [12]–[15] is needed to optimize their volume, to evaluate electrodynamics forces [16], to estimate their temperature [17], or to analyse the environmental magnetic-field pollution that they produce [18]. Unfortunately, explicit equations for the ac resistance and internal inductance per-unit length are only available in case of conductors with circular or elliptical cross-section, and no explicit solutions have been found for rectangular conductors [1], [19]–[21]. Therefore, analytical and numerical models must be used instead [11], [22].

Different numerical methods have been proposed in the technical literature for obtaining the current density in rectangular conductors, taking into account both skin and proximity effects. On the one hand, analytical models of the bus bar conductors have been proposed in [11] for evaluating the electrodynamic forces in a bus bar system, in [23], using a far field/near field analysis, and in [10], using approximate triple integrals for obtaining the magnetic field produced by a three-phase bus duct system. Nevertheless, these models are either approximated, or must be used in combination with numerical approaches, as for example in [15], [24], where the problem is formulated into a set of integral equations, which kernel is expressed analytically in the quasi-static regime, but the solution is found numerically using the method of moments (MoM). On the other hand, numerical methods have been used for obtaining the frequency dependent parameters of the bus bar conductors. The finite element method (FEM) has been used in [17] for the magnetic and thermal simulation of bus bar conductor, in [25] for analysing the solenoidal current flow in rectangular filamentary conductors, and in [6] for cables on a tray or in an enclosing pipe. Nevertheless, as [26] points out, the resulting finite elements global system matrix is not sparse in case of skin effect problems, which

This work was supported by the Spanish "Ministerio de Ciencia, Innovación y Universidades (MCIU)", the "Agencia Estatal de Investigación (AEI)" and the "Fondo Europeo de Desarrollo Regional (FEDER)" in the framework of the "Proyectos I+D+i - Retos Investigación 2018", project reference RTI2018-102175-B-I00 (MCIU/AEI/FEDER, UE). The authors are with the Institute for Energy Engineering, Universitat Politècnica de València, Valencia, Spain (e-mail: jmroman@die.upv.es, rupucpa@die.upv.es, asapena@die.upv.es, jorburva@die.upv.es, cartersa@etsii.upv.es, mpineda@die.upv.es, mriera@die.upv.es).

implies high memory requirements and solving times. Reduced order models, such as the proper generalized decomposition approach [14], [21] can alleviate this problem, and offer the possibility of parametric determination of cable properties at a negligible added computational cost. An alternative fast numerical method to model skin and proximity effects consists in replacing the conductors by equivalent longitudinal currents on their surfaces, and building a surface admittance matrix (via a differential surface admittance operator [27], [28], or a Dirichlet to Neumann operator [29], [30]), which is combined with an integral-equation approach to obtain the resistance and inductance matrices of multiconductor transmission lines.

A simpler numerical method for the analysis of conductors with non-circular shapes consists in the subdivision of each conductor into subconductors, small enough so that uniform current density can be assumed in each of them [31]–[33], which reduces the problem to a simple network representation, as in the partial element equivalent circuit (PEEC) method [34]. The main difficulty that arises in this approach, which is addressed in the present work, is that the inductance matrix of the resulting network is a dense one, because it contains the mutual inductances between all the subconductors. To represent accurately the skin and proximity effects, the dimensions of these subconductors must be smaller than the skin depth, which decreases with the square root of frequency. Therefore, a great number of small subconductors are needed at high frequencies, which results in a huge inductance matrix and renders the network intractable. Diverse solutions have been proposed in the technical literature to solve this problem. In [35] the network is solved via the normal-mode theory of current flow in linear conductors of rectangular shape, by finding a set of spatial distributions of current that form an orthogonal set, which reduces the inductance matrix to a diagonal one. This method has been extended in [12] to conductors of arbitrary shape, and in [36] to polyphase systems. In [37], [38], subconductor currents are obtained as power series expansions in frequency, and each element of the impedance per unit length (p.u.l.) matrix is obtained as a ratio of power expansions in frequency. Using the same formulation, but avoiding the use of series expansions, in [39] the calculation of the subconductor currents is avoided using the partial inductance concept [40]. The p.u.l. impedance matrix for the system of conductors is obtained by forming appropriate row and column sums over the segment matrix, so that an explicit calculation of the segment currents is bypassed. The partial inductance approach has been applied also to the analysis of conductors in [10], [11], [13], [40]–[43]. Other methods, such as those based on induced voltage instead of partial inductances, have been also proposed recently [44]. Nevertheless, both in partial inductance and in induced voltage methods, the problem of dealing with huge inductance matrices when the size of the subconductors is small remains. To alleviate the problem of the huge size of the inductance matrix, several works propose matrix partitioning techniques [32], non-uniform grids [34], and other works propose to use subconductors with different cross-sections, as a way to reduce the total number of elements: annular segments with frequency dependent radii in [22], trapezoidal, elemental shapes [31], or square subconductors with different size depending on their position inside the conductor [5]. These proposals achieve a reduction of the inductance matrix size, at the expense of a much greater complexity on the calculation of its elements, because different formulas are needed for each shape [31].

The solution proposed in this work follows the partial inductance approach, using simple, constant size square subconductors, and develops a novel technique for avoiding the assembly of the inductance matrix, and its multiplication with the current vector. This product is calculated instead in the spatial frequency domain, using the convolution theorem, which reduces it to an element-wise product of the current vector and the magnetic vector potential (MVP) generated by a filament with unitary current. This technique has been used in other fields, such as in the calculation of the far field effect of currents in semiconductors [45], or for solving large-scale electromagnetic scattering and radiation problems [46], but, up to the best of the authors' knowledge, it is the first time that it is applied to the analysis of busbar systems. The use of the fast Fourier transform (FFT) for implementing this technique makes this approach very fast and simple to apply.

The structure of the paper is as follows. Section II presents briefly the method of subdivision of conductors in filamentary subconductors, and establishes the matrix equation of the busbar system in a current-driven approach. In Section III, the proposed method to solve this equation in the spatial frequency domain, using the convolution theorem and the FFT, is presented. The results obtained in Section IV are compared with other related works in Section V, and validated with a FEM model in Section VI. Section VII presents the conclusions of this work.

II. Numerical Model of the Three Phase Busbar System

The busbar system considered in this work has three phase bars (L_1, L_2, and L_3) plus a neutral one (N), as depicted in Fig. 1, left. The bars are considered to have an infinite length, directed along the z axis [43]. The dimensions of the system are a=12 mm, b=100 mm, and d=24 mm. All the bars are made of copper (conductivity σ=58 MS m^{-1}). The currents are assumed sinusoidal, with a frequency f=50 Hz.

A. Equation of the Current Inside a Bar

The equation of the current inside a bar is formulated starting from the Maxwell equation,

$$\nabla \times \mathbf{E} = -\frac{\partial \mathbf{B}}{\partial t} \tag{1}$$

where $\mathbf{E}$ is the electric intensity vector, and $\mathbf{B}$ is the magnetic flux density vector. Using the scalar potential V, and the magnetic vector potential (MVP), $\mathbf{A}$, defined by the relation $\mathbf{B} = \nabla \times \mathbf{A}$, (1) can be expressed as [43]

$$\mathbf{E} = -\nabla V - \frac{\partial \mathbf{A}}{\partial t} \tag{2}$$

Applying also the relation $\mathbf{E} = \sigma \mathbf{J}$, where $\mathbf{J}$ is the current density vector, (2) becomes

$$-\nabla V = \frac{\mathbf{J}}{\sigma} + \frac{\partial \mathbf{A}}{\partial t} \tag{3}$$

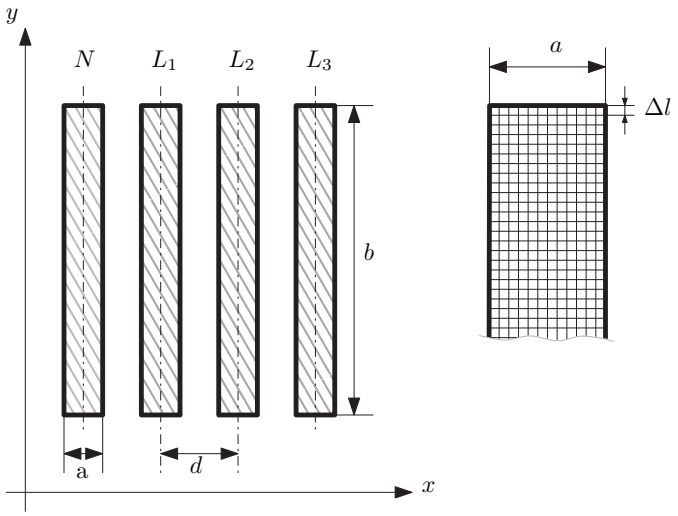

Fig. 1. Busbar system considered in this work (left): three phase bars plus a neutral one, with a=12 mm, b=100 mm, and d=24 mm. All the bars are made of copper (conductivity σ=58 MS m^{-1}). The currents are assumed sinusoidal, with a frequency of f=50 Hz. The subdivision of the bars into filamentary subconductors, with a square cross section of side length Δl=1 mm, is shown in a zoomed view on the right.

As the currents are assumed to flow only in the z direction, both $\mathbf{J}$ and $\mathbf{A}$ are solely z-directed. Therefore, they will be denoted as scalars, J and A. Besides, on the cross-section of a given bar k, the voltage gradient is constant, and (3) becomes

$$(-\nabla V)_k = \frac{J(x,y)}{\sigma_k} + \frac{\partial A(x,y)}{\partial t} \tag{4}$$

where (x, y) are the coordinates of the cross-section points of the kth bar, and σ_k is its conductivity. Assuming time harmonic excitation, with a time dependence $e^{j\omega t}$ ($\omega = 2\pi f$), (4) reduces to the phasor form

$$(-\nabla V)_k = \frac{J(x,y)}{\sigma_k} + j\omega A(x,y) \tag{5}$$

The integration of (5) in the z-direction, along the conductors, between two points separated 1m, gives

$$\int_z^{z+1} (-\nabla V)_k \, dz = \int_z^{z+1} \frac{J(x,y)}{\sigma_k} \, dz + \int_z^{z+1} j\omega A(x,y) \, dz \tag{6}$$

and, therefore,

$$(V_z - V_{z+1})_k = \nabla V_k = \frac{J(x,y)}{\sigma_k} + j\omega A(x,y) \tag{7}$$

where ∇V_k is the p.u.l. voltage drop along the kth bar.

The value of the MVP at the point with coordinates (x,y), $A(x, y)$ in (7), can be obtained from all the current densities in the whole planar cross-section of the busbar system S, located at any position (ξ, η) in this domain, as a function of their distance to the point (x, y), as [20], [43], [47]

$$A(x,y) = \frac{\mu_0}{2\pi} \iint_S J(\xi,\eta) \ln \frac{1}{\sqrt{(x-\xi)^2 + (y-\eta)^2}} \, d\xi \, d\eta + C \tag{8}$$

where C is an arbitrary constant that depends on the potential reference [47], and can be taken as zero if the total sum of the currents is zero, as in the busbar system of Fig. 1.

In (8) $\mu_0 = 4\pi 10^{-7}$ (H·m^{-1}) is the magnetic permeability of the vacuum, which is assumed to be the same at every point of the busbar system. The presence of magnetic materials with a high permeability could be considered by replacing them with fictitious currents using the method of images, but this case has not been considered in the present work.

B. Subdivision of the Bars into Filamentary Subconductors

To obtain the current density applying (7) and (8), each bar is subdivided into smaller subconductors, so small that the current density can be assumed as uniform inside each of them. The following assumptions are used:

- The bars are considered composed of parallel filaments, all with the same square cross section.
- The current flows only longitudinally in the subconductors. No currents are assumed to flow between them.
- Uniform current density in each subconductor.
- Uniform, constant resistivity within each bar.
- Non-magnetic materials, with a relative magnetic permeability equal to one.

The cross-sectional area of the elemental conductors must be small enough to neglect the skin effect, so considering a uniform current density [10]. The skin depth is given by $\delta = \sqrt{2/(2\pi f \mu \sigma)}$, where f is the frequency, μ is the magnetic permeability and σ is the conductivity. In this work $f = 50$ Hz, and, with copper conductors, $\delta = 9.3$ mm. As in [11], the criterion used for selecting the size of the subconductors is that their diagonal is no greater than δ, which represents a thickness lower than 6 mm in this work. The subconductor thickness has been chosen as $\Delta l = 1$ mm (see Fig. 1, right), fully complying with this limitation, which gives $N_s = 4800$ subconductors in this busbar system.

For easy of notation, from now on, the number of bars will be denoted by N_b and the number of subconductors per bar as N_c. In this case, $N_b = 4$ and $N_c = N_s/N_b = N_s/4$, which is the same for all the bars. Busbar systems with a different number of subconductors in each bar can be treated also with the proposed approach. The conductor i of bar k ($k = 0..N_b - 1$, $i = 0..N_c - 1$) will be denoted as conductor ki, and its cross-sectional surface will be denoted as S_{ki}.

Eq. (7) can be integrated over the cross-sectional surface of each subconductor ki as

$$\iint_{S_{ki}} \nabla V_k \, dx \, dy = \iint_{S_{ki}} \frac{J(x,y)}{\sigma_k} \, dx \, dy + \iint_{S_{ki}} j\omega A(x,y) \, dx \, dy \tag{9}$$

giving

$$\nabla V_k \cdot \Delta s = \frac{J_{ki}}{\sigma_k} \cdot \Delta s + j\omega \iint_{S_{ki}} A(x,y) \, dx \, dy \tag{10}$$

where $\Delta s = \Delta l^2$ is the cross-sectional area of a subconductor, and J_{ki} is the current density in subconductor ki. Eq. (10) can be rewritten as

$$\nabla V_k = R_k \cdot I_{ki} + j\omega \frac{1}{\Delta s} \iint_{S_{ki}} A(x,y) \, dx \, dy \tag{11}$$

where $R_k = 1/(\sigma_k \cdot \Delta s)$ is the p.u.l resistance of a subconductor of bar k, and $I_{ki} = J_{ki} \cdot \Delta s$ is the current in subconductor ki. The value of the MVP at a point with coordinates (x,y) in (11), $A(x, y)$, can be obtained adding the contributions of the currents through all the subconductors, using (8), as

$$A(x,y) = \\ = \sum_{\ell=0}^{N_b-1} \sum_{j=0}^{N_c-1} \frac{\mu_0}{2\pi} \iint_{S_{\ell j}} J(\xi,\eta) \ln \frac{1}{\sqrt{(x-\xi)^2+(y-\eta)^2}} \, d\xi \, d\eta \tag{12}$$

Defining he geometrical mean distance (GMD) $d_{ki,\ell j}$ between subconductors ki and ℓj as [43], [48]

$$\ln d_{ki,\ell j} = \frac{1}{\Delta s^2} \iint_{S_{ki}} \iint_{S_{\ell j}} \ln \sqrt{(x-\xi)^2+(y-\eta)^2} \, d\xi \, d\eta \, dx \, dy \tag{13}$$

and replacing (12) and (13) in (11) gives

$$\nabla V_k = R_k \cdot I_{ki} + j\omega \sum_{\ell=0}^{N_b-1} \sum_{j=0}^{N_c-1} \frac{\mu_0}{2\pi} \ln \frac{1}{d_{ki,\ell j}} \cdot I_{\ell j} \tag{14}$$

In case of $ki = \ell j$, (13) gives the geometric mean radius (GMR) of subconductor ki. The GMD between to subconductors can be approximated by their centre-to-centre distance, with an error in the worst case (adjacent subconductors) of 0.655% [31]. The GMR of a square subconductor of side length Δl is given within 0.13% by the formula $d_{ki,ki} = 0.44705 \cdot \Delta l$ [48].

In (14) the term $\frac{\mu_0}{2\pi} \ln \frac{1}{d_{ki,\ell j}}$ represents the partial inductance between subconductors ki and lj, $L_{ki,\ell j}$ [20]. It is defined as the ratio of the magnetic flux penetrating the rectangular surface between the subconductor ki and infinity, per unit length, to the current in subconductor ℓj, $I_{\ell j}$, which produces that flux. Using partial inductances, (14) can be expressed as

$$\nabla V_k = R_k \cdot I_{ki} + j\omega \sum_{\ell=0}^{N_b-1} \sum_{j=0}^{N_c-1} L_{ki,\ell j} \cdot I_{\ell j} \tag{15}$$

with

$$L_{ki,\ell j} = \frac{\mu_0}{2\pi} \ln \frac{1}{d_{ki,\ell j}} \tag{16}$$

The systems of equations (15) can be expressed using matrix notation as

$$\nabla \mathbf{V} = (\mathbf{R} + j\omega \mathbf{L}) \cdot \mathbf{I} = \mathbf{Z} \cdot \mathbf{I} \tag{17}$$

where $\nabla \mathbf{V}$ is the vector of the N_s p.u.l. voltage drops along the subconductors, $\mathbf{I}$ is the vector of the N_s subconductor currents, $\mathbf{R}$ is an $N_s \times N_s$ diagonal matrix with all its elements equal to $\frac{1}{\sigma \cdot \Delta s}$ (in this work all the bars have the same conductivity), and $\mathbf{L}$ is an $N_s \times N_s$ symmetrical matrix that contains the partial inductances between the subconductors given by (16).

C. Current Driven Formulation

Two different formulations can be established for the busbar system, a current-driven and a voltage-driven one [11]. In this work, a current problem has been chosen: the total current in each bar is specified, being the drop of voltage along all the subconductors of a given bar the same, but unknown. To establish the matrix equation of this problem, the numbering of the subconductors in (15) is made sequentally by bars: the first N_c subconductors belong to the neutral bar N, the next N_c subconductors belong to phase bar L_1, and so on. Using this numbering schema, the current driven problem is formulated adding four more equations to (17), corresponding to the imposed currents in the bars, what results in the following matrix equation,

$$\left[\begin{array}{c|c} \mathbf{Z} & -\mathbf{N}^T \\ \hline \mathbf{N} & 0 \end{array}\right] \left[\begin{array}{c} \mathbf{I} \\ \hline \nabla \mathbf{V} \end{array}\right] = \left[\begin{array}{c} 0 \\ \hline \mathbf{I_b} \end{array}\right] \tag{18}$$

where $\nabla \mathbf{V} = [\nabla V_N, \nabla V_{L1}, \nabla V_{L2}, \nabla V_{L3}]^t$ (^{t} stands for the transpose operator) is the p.u.l drop of voltage along each bar, $\mathbf{I_b} = [I_N, I_{L1}, I_{L2}, I_{L3}]^t$ are the prescribed bar currents, and $\mathbf{N}$ is a matrix of dimensions $4 \times N_s$ which adds the currents of the $N_s/4$ subconductors of each bar to give the total bar current, as

$$\left[\begin{array}{c|c|c|c} \overbrace{1 \ \ldots \ 1}^{N_s/4} & 0 & 0 & 0 \\ \hline 0 & 1 \ \ldots \ 1 & 0 & 0 \\ \hline 0 & 0 & 1 \ \ldots \ 1 & 0 \\ \hline 0 & 0 & 0 & 1 \ \ldots \ 1 \end{array}\right] \tag{19}$$

The linear system (18) must be solved to find the current in all the subconductors, $\mathbf{I}$, plus the drops of voltage along each bar, $\nabla \mathbf{V}$. The problem is that (18) is a very large system, because the matrix $\mathbf{L}$ in (17) is dense and huge. In the busbar system considered in this work, its size is $N_s \times N_s = 4800 \times 4800$ elements, that is, it scales quadratically with the number of subconductors. And it is a dense matrix. A possible simplification is to zero the entries of the inductance matrix corresponding to subconductors that are separated by a long distance, because their effects are negligible, but this approach may led to an inductance matrix without a positive definiteness property [49].

The most usual approach for solving large system of equations such as (18) is not a direct solution, based on Gaussian elimination, which is very slow in this case. Instead, iterative methods are used, which produce an approximate solution of vectors $\mathbf{I}$ and $\nabla \mathbf{V}$ after a finite number of iterations, such as the generalized minimal residual method (GMRES) used in this work. Starting with zero vectors $\mathbf{I}$ and $\nabla \mathbf{V}$, the following process is used for solving (18):

1) Compute the residual norm res as the difference between the right-hand side and the left-hand side of (18).
2) Compare the residual against a specified tolerance tol. If $res <= tol$, the computation ends.
3) If the maximum number of iterations has not been reached, update the magnitude and direction of the

vectors $\mathbf{I}$ and $\nabla\mathbf{V}$ based on the value of the residual, and return to Step 1.

Step 1 of this process requires a costly matrix-vector multiplication, $\mathbf{Z}\cdot\mathbf{I}$, with a computational complexity $\mathcal{O}(N_s^2)$, which must be performed at each iteration. Nevertheless, there is a way to avoid forming the entire coefficient matrix $\mathbf{Z}$, making the calculation much more efficient. It consists in replacing the matrix-vector multiplication $\mathbf{Z}\cdot\mathbf{I}$ by a convolution in the spatial domain, with a much lower computational complexity, as explained in the next Section.

III. Proposed Method for Obtaining the Current Density in the Busbar System through the FFT and the Convolution Theorem

Using the concept of partial inductance, the summation term in (14), or each entry of the matrix-vector multiplication $\mathbf{L}\cdot\mathbf{I}$ in (17), can be expressed as

$$\psi_{ki} = \sum_{\ell=0}^{N_b-1}\sum_{j=0}^{N_c-1} L_{ki,\ell j}\cdot I_{\ell j} \tag{20}$$

where ψ_{ki} represents the flux linkage of subconductor ki, that is, the total magnetic flux penetrating the rectangular surface between the subconductor ki and infinity, per-unit length, generated by all the busbar currents. The flux linkages of all the subconductors can be represented using a vector $\mathbf{\Psi}$ with the N_s flux linkages of the subconductors, and (20) can be expressed in matrix form as

$$\mathbf{\Psi} = \mathbf{L}\cdot\mathbf{I} \tag{21}$$

The main idea of the method proposed in this work is to use a uniform grid to mesh the busbar system domain, so that the discrete FFT can be applied to calculate (21), avoiding the costly matrix-vector multiplication $\mathbf{L}\cdot\mathbf{I}$. This requires meshing the whole domain, including the non-conducting regions, as shown in Fig 2. Paradoxically, this approach, which increases the number of points compared with the usual approach of meshing only the cross-sections of the bars, results in a great reduction of computational complexity.

The uniform grid used in this work is aligned with the centres of the subconductors, and must include all the bars, as shown in Fig 2. The currents and flux linkages of each subconductor are assigned to the grid point that coincides with its centre. The grid cells have the same dimensions than the elementary subconductors. For the busbar system considered in this work, the minimum grid that contains all the busbar subconductor centres has $N_x = (3d+a)/\Delta l = 84$ points in the x direction, and $N_y = b/\Delta l = 100$ points in the y direction, as depicted in Fig. 2. The spatial (x, y) coordinates of the (m, n) grid node are $(m\Delta l, n\Delta l)$.

Nevertheless, for correctly applying the convolution theorem, the minimal grid of Fig. 2 must be zero-padded in each direction, as shown in Fig. 3. The final size of the uniform grid will be $N_g = (2N_x-1)\times(2N_y-1)$. On this spatial grid, three matrices are defined:

- The current matrix $\mathbf{I_g}$. Its element $I_g(m,n)$ is the current in the subconductor located at the grid node (m,n) (it will be zero outside the bars).

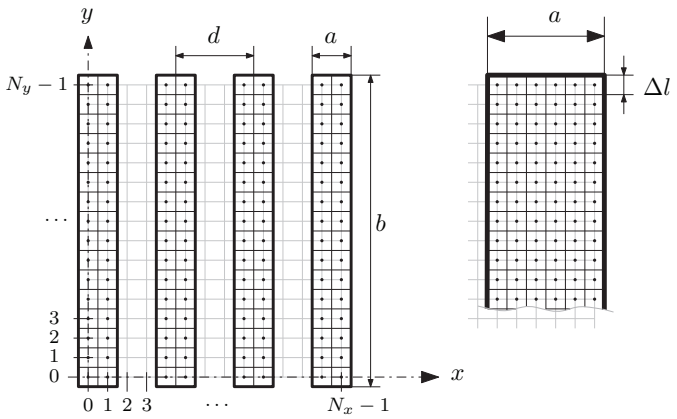

Fig. 2. Uniform grid (gray color), aligned with the subconductor centres (black dots), for the busbar system considered in this work. It has $N_x = (3d+a)/\Delta l = 84$ points in the x direction, and $N_y = b/\Delta l = 100$ points in the y direction.

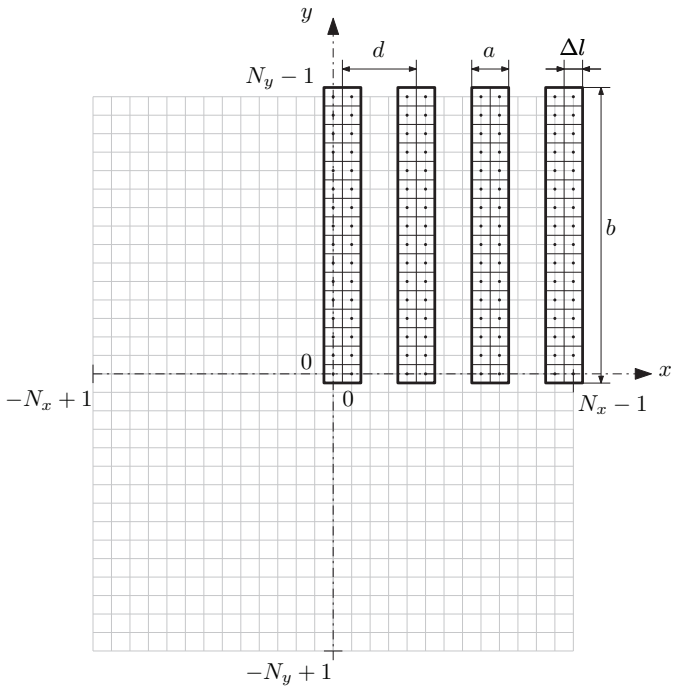

Fig. 3. Extended grid, needed to apply the convolution theorem. The original grid depicted in Fig. 2 is zero-padded in both directions, for correctly applying the circular convolution.

- The flux linkage matrix $\mathbf{\Psi_g}$. Its element $\Psi_g(m,n)$ is the flux linkage (20) of the subconductor located at the grid node (m,n).
- The partial inductance matrix $\mathbf{L_g}$. Its element $L_g(m,n)$ is the partial inductance between two subconductors, one located at the origin of coordinates and the other one at the grid node (m,n). From (16),

$$L_g(m,n) = \begin{cases} \frac{\mu_0}{2\pi}\ln\frac{1}{0.44705\cdot\Delta l} & \text{if } m=n=0 \\ \\ \frac{\mu_0}{2\pi}\ln\frac{1}{\sqrt{m^2+n^2}\cdot\Delta l} & \text{otherwise} \end{cases} \tag{22}$$

Fig. 4 represents $L_g(m,n)$ (22) in the grid used in Fig. 3. It is worth mentioning that matrix $\mathbf{L_g}$ only depends

on the grid geometry, and not on the position of the bars in the grid, which gives a great flexibility to the proposed method. Therefore, it can be calculated once for a given grid region, and is valid for any distribution of the bars inside this planar region.

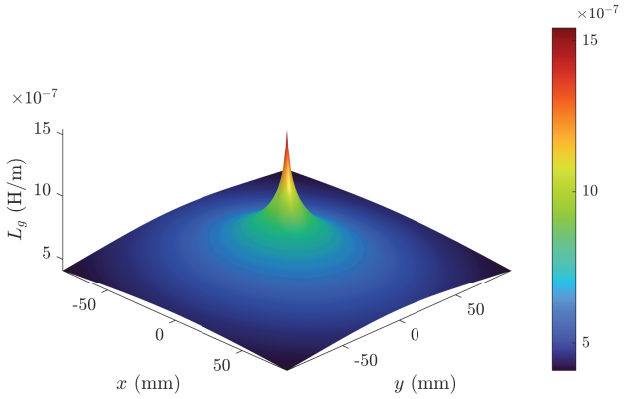

Fig. 4. Partial inductance matrix $\mathbf{L_g}$ corresponding to the busbar system of Fig. 63. Its element $L_g(m,n)$ (22) is the partial inductance between two subconductors, one located at the origin of coordinates and the other one at the grid node (m,n).

Using matrices $\mathbf{\Psi_g}$, $\mathbf{I_g}$, and $\mathbf{L_g}$, and taking into account that the subconductor currents are restricted to the first quadrant, (20) can be formulated in grid coordinates as

$$\psi_g(m,n) = \sum_{p=0}^{N_x-1} \sum_{q=0}^{N_y-1} L_g(m-p, n-q) \cdot I_g(p,q) \qquad (23)$$

The direct evaluation of (23) requires a costly matrix-vector multiplication, even greater than the original one (17). Nevertheless, thanks to the regularity of the newly defined spatial grid of Fig. 3, (23) is the expression of the 2D convolution ($*$) of matrices $\mathbf{L_g}$ (which is is a Toeplitz circulant matrix) and $\mathbf{I_g}$, as

$$\mathbf{\Psi_g} = \mathbf{L_g} * \mathbf{I_g} \qquad (24)$$

Exploiting this Toeplitz property [46], the convolution theorem can be applied, and the costly evaluation of (23) can be replaced by a simple element-by-element product of the Fourier transforms of the small spatial matrices $\mathbf{L_g}$ and $\mathbf{I_g}$, implemented in a very efficient way using the FFT (and its inverse, the IFFT), as [45]

$$\mathbf{\Psi_g} = \text{IFFT}(\text{FFT}(\mathbf{L_g}) \cdot \text{FFT}(\mathbf{I_g})) \qquad (25)$$

Therefore, the proposed method for obtaining the right hand side of (23), $\mathbf{Z} \cdot \mathbf{I}$, given the vector of subconductor currents and voltages $[\mathbf{I} \ \nabla\mathbf{V}]^t$, is the following one:

1) The subconductor currents contained in vector $\mathbf{I}$ are mapped to the elements of matrix $\mathbf{I_g}$ corresponding to the location of each subconductor in the uniform grid.
2) The matrix $\mathbf{\Psi_g}$, which contains the flux linkages at each node of the grid, is obtained using (25).
3) The vector $\mathbf{\Psi}$, which contains the flux linkages of each subconductor, is assembled by collecting the elements of $\mathbf{\Psi_g}$ at the bars positions on the grid.
4) The first N_s rows of the right hand side of (17), corresponding to the residuals of voltages in the N_s subconductors, are calculated using the vector $\mathbf{\Psi}$ as $\mathbf{Z} \cdot \mathbf{I} - \nabla\mathbf{V} = 1/(\sigma \cdot \Delta s)\mathbf{I} + j\omega\mathbf{\Psi} - \nabla\mathbf{V}$.
5) The last four rows of the right hand side of (17), corresponding to the total currents in each bar $\mathbf{I_b}$, are calculated by adding all the currents of the subconductors belonging to each bar.

This method has been programmed as a Matlab function (`PropFun`), whose pointer is passed as an argument to the iterative solver (GMRES), along with the right hand side of (18), $\mathbf{b}$, as `gmres(@PropFun,b,[],1e-6,100)`.

A problem associated with the use of the FFT in (25) is that it results in a periodic frequency domain representation of matrix $\mathbf{L_g}$. This means that $\mathbf{L_g}$ wraps around the grid edges when doing the convolution. For example, for evaluating the flux linkages of any subconductor produced by a subconductor located in the upper-right corner ($p = N_x - 1, q = N_y - 1$) in (23), the peak of $\mathbf{L_g}$ is shifted to the upper-right corner, wrapping around the edges, as seen in Fig. 5. The partial inductances to everything other than the upper-right quadrant are incorrect, but it does not matter since the currents in these other quadrants are zero. This justifies the need of zero-padding the original busbar grid (Fig. 2) to obtain the grid of Fig. 3.

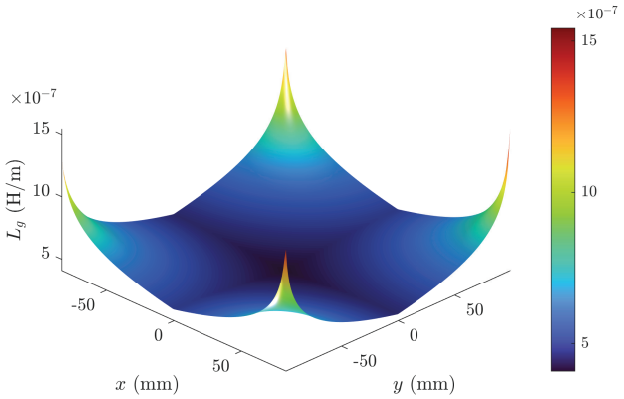

Fig. 5. Partial inductance matrix $\mathbf{L_g}$ shifted by $(N_x - 1, N_y - 1)$ during the application of (23), to evaluate the flux linkages produced by a subconductor located in the upper-right corner. The partial inductances to everything other than the upper-right quadrant are incorrect, but it does not matter since the currents in these other quadrants are zero.

IV. Current Density in the Busbar System Obtained with the Proposed Method

The busbar system has been simulated using a 2.5 kA (RMS) balanced three-phase current system. The modulus of the current density obtained using the proposed method has been represented in Fig. 6 as a 2D plot, and in Fig. 7, using a 3D view to better display the non-uniform current density in each bar.

The modulus of the current density along two horizontal lines of the busbar system have been represented in Fig. 8: one at middle of the bars, $y = b/2 = 50$ mm (blue line), and other one near the top edge $y = 0.99 \cdot b = 99$ mm (red line). It

can be observed a strong displacement of the current towards the bar edges, even at a rated frequency of 50 Hz.

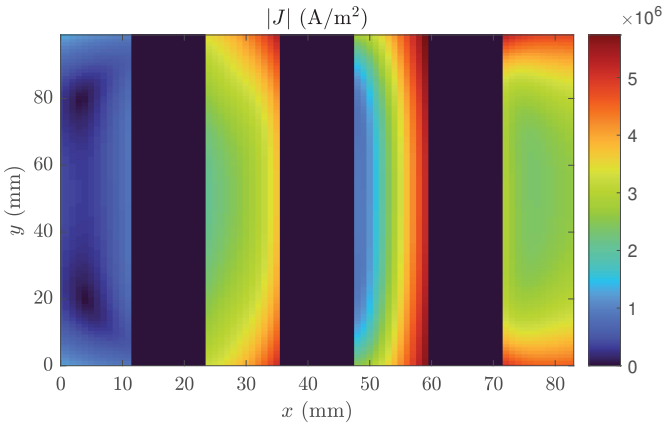

Fig. 6. Modulus of the current density in the analysed busbar system for a balanced three-phase current system of 2.5 kA.

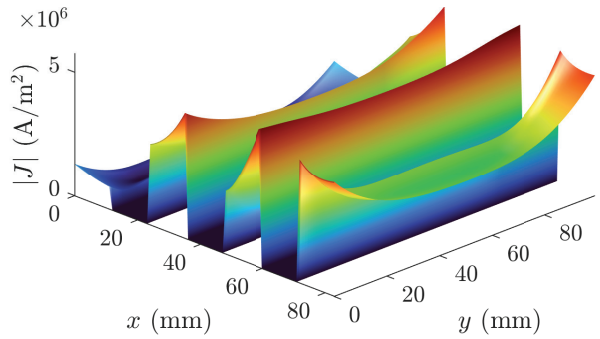

Fig. 7. 3D view of the modulus of the current density in the analysed busbar system for a balanced three-phase current system of 2.5 kA.

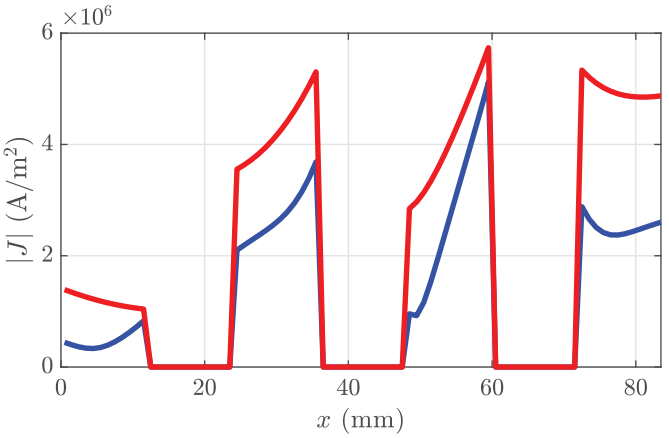

Fig. 8. Modulus of the current density along two horizontal lines: a middle line, at $y = 50$ mm (blue line), and a line close to the top edge of the bars, at $y = 99$ mm (red line), for a balanced three-phase current system of 2.5 kA.

V. Comparison with Other Numerical Methods

For comparative purposes, the linear system (18) has been solved both with the proposed approach and with other numerical methods that rely on the matrix-vector multiplication, a direct solver and an iterative solver, using GMRES. The computer platform used is detailed in the Appendix. The linear system (18) can be expressed in compact form as

$$\mathbf{M} \cdot \mathbf{x} = \mathbf{b} \tag{26}$$

where

$$\mathbf{M} = \left[\begin{array}{c|c} \mathbf{Z} & -\mathbf{N}^T \\ \hline \mathbf{N} & 0 \end{array}\right] \tag{27}$$

is a square matrix with $(N_s + 4) \times (N_s + 4)$ elements, $\mathbf{x} = [\mathbf{I} \quad \nabla\mathbf{V}]^t$, and $\mathbf{b} = [0 \quad \mathbf{I_b}]^t$ are column vectors with $N_s + 4$ elements.

Table I shows the memory usage (in GB) and the times needed to build and solve the problem (wall times measured with Matlab function `timeit`), obtained when solving (26) using a direct solver (`x = M\b` in Matlab code), and an iterative solver based on the direct matrix-vector multiplication $\mathbf{M} \cdot \mathbf{x}$ (`x=gmres(M,b,[],1e-6,100)` in Matlab code). Besides, the problem has been solved with increasing spatial resolutions, for three different values of the cell size Δl (1 mm, 0.5 mm, 0.25 mm), each one halving the previous value. As shown in Table I, the last value of Δl leads to a huge matrix $\mathbf{M}$, which makes it impossible to solve it with the computer platform given in the Appendix.

TABLE I
Computing resources needed for solving (26) with a direct and an iterative methods, for increasing spatial resolution

Δl (mm)	Size of $\mathbf{M}$ (GB)	Time to build the problem (s)	Time to solve the problem (s)	
			Direct solver	Iterative solver
1	0.18	3.34	2.61	0.45
1/2	2.95	66.45	155.01	6.09
1/4	47.19	Not enough memory error		

The same problem has been solved using the proposed method (`x=gmres(@PropFun,b,[],1e-6,100)` in Matlab code, where `PropFun` is the function that implements the convolution based method proposed in this work). In this case, matrix $\mathbf{L_g}$ is the most demanding in terms of memory requirements. Table II shows its size (in MB), and the time needed to build and solve the problem (26) using the proposed method, for the same increasing spatial resolutions presented in Table I. The total times (time to build plus time to solve) obtained from Table I and Table II have been represented in Fig. 9.

A direct comparison of the results presented in Table I and Table II shows that, in the proposed method, the memory requirements have been reduced up to four orders of magnitude, the time to build the problem has been reduced two orders of magnitude, and the time to solve the problem has been reduced up to one order of magnitude. Besides, with the computer platform given in the Appendix, the proposed method is able to solve problems that are intractable with

TABLE II
COMPUTING RESOURCES NEEDED FOR SOLVING (26) WITH THE PROPOSED METHOD, FOR INCREASING SPATIAL RESOLUTION

Δl (mm)	Number of conductors	Size of $\mathbf{L_g}$ (MB)	Time to build (s)	Time to solve (s)
1	4800	0.27	0.002	0.17
1/2	19200	1.07	0.006	0.50
1/4	76800	4.29	0.021	1.90
1/8	307200	17.19	0.097	7.58
1/16	1228800	68.77	0.399	49.35
1/32	4915200	275.16	1.711	219.8

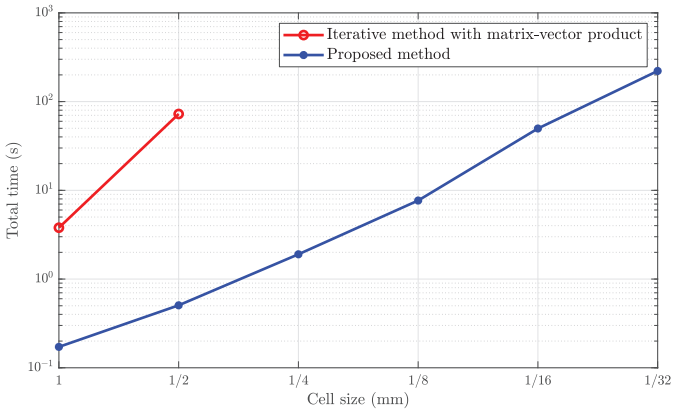

Fig. 9. Total time, in logarithmic scale, for solving the problem (26) with the proposed method (blue line) and with an iterative solver based on the direct matrix-vector multiplication (red line), for increasing spatial resolutions. Only the first two points can calculated using the direct matrix-vector multiplication due to its huge memory requirements at high spatial resolutions. The proposed method overcomes this limitation, and is much faster for a given cell size.

an iterative solver that implements directly the matrix-vector multiplication $\mathbf{M}\cdot\mathbf{x}$, such as using high spatial resolution, what allows the simulation at high frequencies, or solving much larger problems, with a given cell size.

VI. VALIDATION WITH A FEM MODEL

To further validate the proposed approach, the busbar system of Fig. 1 has been simulated using a standard 2D FEM method for magnetics, FEMM [50]. This problem has no natural outer boundary. To approximate this open boundary problem, an asymptotic boundary condition is used: a circular outer boundary enclosing the busbar system, with a radius $r = b$ has been defined, and the "IABC Open Boundary" tool available in FEMM has been applied to it, with a Dirichlet boundary condition (MVP=0).

Fig. 10 presents the modulus of the current density computed with FEM, which agrees with the current density obtained with the proposed method, depicted in Fig. 6.

In Fig. 11, the modulus of the current density along a horizontal line in the middle of the bars, at $y = 50$ mm, calculated with FEM (solid, blue line) and with the proposed method (red triangles) is depicted, and in Fig. 12, the same comparison is presented along a horizontal line close to the top edge of the bars, at $y = 99$ mm. These results show a very good agreement between both methods.

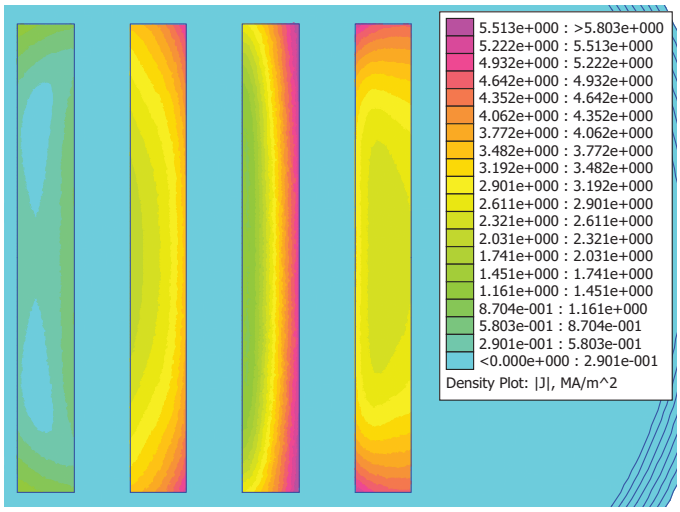

Fig. 10. Current density for a balanced three-phase current system of 2.5 kA, calculated with FEM.

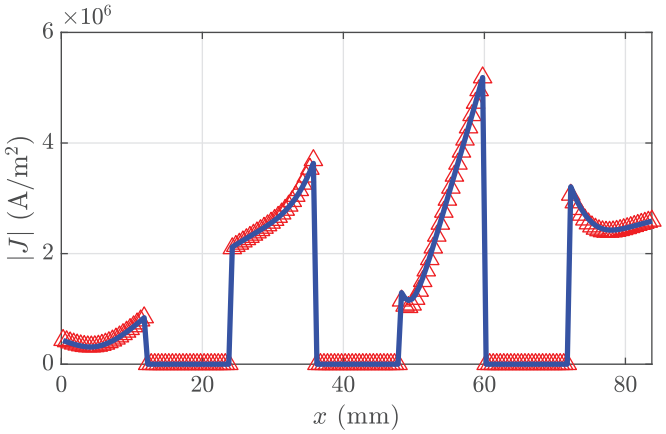

Fig. 11. Modulus of the current density for a balanced three-phase current system of 2.5 kA, along a horizontal line in the middle of the bars, at $y = 50$ mm, calculated with FEM (solid, blue line) and with the proposed method (red triangles).

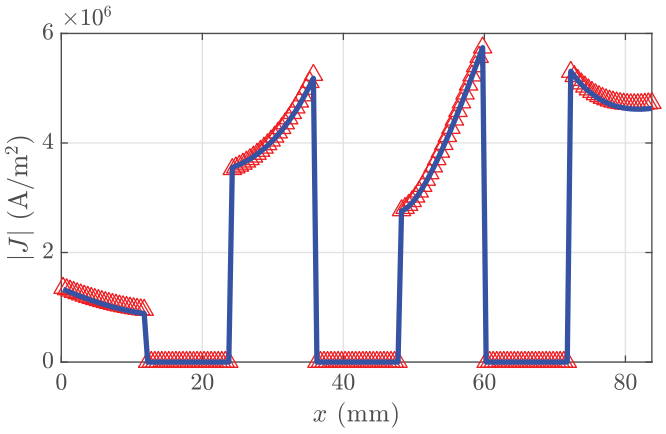

Fig. 12. Modulus of the current density for a balanced three-phase current system of 2.5 kA, along a horizontal line close to the top edge of the bars, at $y = 99$ mm, calculated with FEM (solid, blue line) and with the proposed method (red triangles).

The maximum errors (in %) along the horizontal lines at the middle and close to the top edge of the bar, relative to the FEM solution are depicted in Table III, and they have been plotted in Fig. 13, for increasing spatial resolutions. Regarding computing times, the FEM solution requires 3.03 seconds on the computing platform given in the Appendix (with a triangular mesh of 14904 nodes). The times needed to compute the proposed approach in the same computing platform are depicted in Table II, and range between 0.17 seconds for a cell size of 1 mm to 219.8 seconds for a cell size of 1/32 mm. It is worth mentioning that, although the finite elements (FE) model has a great flexibility and speed, and modern-day FE software can deal with the busbar system, the method of subconductors offers a very intuitive and physical description of the problem, uses a very simple orthogonal mesh and can be programmed easily without needing a full FE software. Anyway, both methods cannot be considered as mutually exclusive, and the proposed approach tries to improve one of them, expanding the field of application of the subconductors method to busbar systems that cannot be treated with iterative solvers based on direct matrix-vector multiplication, due to the size of the inductance matrix. In particular, it may be useful for simulating high frequency problems, with a fine spatial resolution, or large busbar systems.

TABLE III
MAXIMUM ERRORS ALONG THE HORIZONTAL LINES AT THE MIDDLE AND CLOSE TO THE TOP EDGE OF THE BAR WITH THE PROPOSED METHOD, RELATIVE TO THE FEM SOLUTION, FOR INCREASING SPATIAL RESOLUTIONS.

Δl (mm)	Maximum error middle line	Maximum error top line
1	5.70 %	3.02 %
1/2	2.81 %	1.65 %
1/4	1.46 %	0.96 %
1/8	0.79 %	0.62 %
1/16	0.48 %	0.45 %
1/32	0.35 %	0.35 %

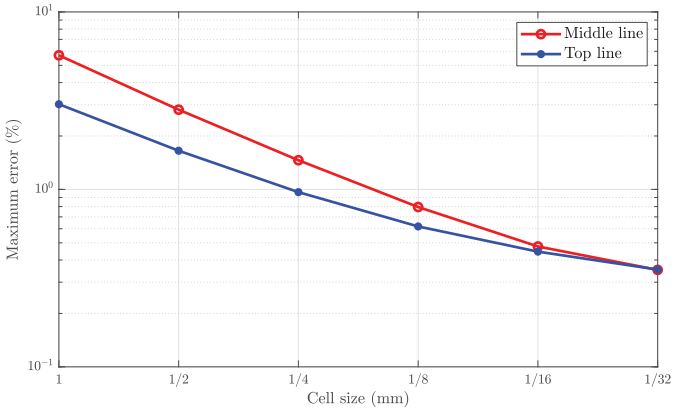

Fig. 13. Maximum relative errors (in logarithmic scale) along the horizontal lines at the middle (red line) and close to the top edge (blue line) of the busbar system with the proposed method, relative to the FEM solution, for increasing spatial resolutions.

VII. CONCLUSIONS

In this work, a novel technique has been presented for obtaining the current density in industrial busbar systems, based on the method of subdivision of the bars in filamentary subconductors. This method allows taking into account both the skin and proximity effects using a simple formulation. Nevertheless, one of its known problems is that it involves a costly matrix-vector multiplication, where the mutual inductances matrix is a dense, huge one, proportional to the number of subconductors squared. The method proposed in this work circumvents this computation by applying the convolution theorem, converting it into a fast element-wise product of small matrices in the spatial frequency domain. This method has been theoretically presented, compared with other numerical methods and validated with a FEM model of an industrial busbar system. It can be easily extended, using the convolution theorem, to the computation of the magnetic fields around the conductors, and of the forces acting between them, which is a work under development.

APPENDIX

Computer features. CPU: Intel Core i7-2600K CPU @ 3.40 GHZ RAM memory: 16 GB, Matlab Version: 9.10.0.1602886 (R2021a).

REFERENCES

[1] V. T. Morgan, "The Current Distribution, Resistance and Internal Inductance of Linear Power System Conductors—A Review of Explicit Equations," *IEEE Transactions on Power Delivery*, vol. 28, no. 3, pp. 1252–1262, 2013.

[2] P. E. Sutherland, "Inductance Effects in Grounding and Bonding for Three-Phase AC Systems," *IEEE Transactions on Industry Applications*, vol. 51, no. 6, pp. 5078–5085, 2015.

[3] Y. Song, E. Ebrahimzadeh, and F. Blaabjerg, "Analysis of High-Frequency Resonance in DFIG-Based Offshore Wind Farm via Long Transmission Cable," *IEEE Transactions on Energy Conversion*, vol. 33, no. 3, pp. 1036–1046, 2018.

[4] M. S. Murthy and G. A. Rasek, "Analytical Determination of Current Distributions in Shielded HV Cables and Ground Systems of Electric Automotive Power Trains," *IEEE Transactions on Electromagnetic Compatibility*, vol. 61, no. 3, pp. 911–918, 2019.

[5] Yaw-Juen Wang and Jung-Hsiang Wang, "Modeling of frequency-dependent impedance of the third rail used in traction power systems," *IEEE Transactions on Power Delivery*, vol. 15, no. 2, pp. 750–755, 2000.

[6] W. L. de Souza, H. de Paula, A. De Conti, and R. C. Mesquita, "Cable Parameter Calculation for Typical Industrial Installation Methods and High-Frequency Studies," *IEEE Transactions on Industry Applications*, vol. 54, no. 4, pp. 3919–3927, 2018.

[7] J. W. Chin, K. S. Cha, J. C. Park, D. M. Kim, J. P. Hong, and M. S. Lim, "Investigation of AC Resistance on Winding Conductors in Slot According to Strands Configuration," *IEEE Transactions on Industry Applications*, vol. 57, no. 1, pp. 316–326, 2021.

[8] A. Mohos, J. Ladanyi, and D. Divenyi, "Methods to ascertain the resistance of stranded conductors in the frequency range of 40 Hz-150 kHz," *Electric Power Systems Research*, vol. 174, p. 105862, 2019. [Online]. Available: https://www.sciencedirect.com/science/article/pii/S0378779619301750

[9] J. Lyu, H. Chen, Y. Zhang, Y. Du, and Q. S. Cheng, "Fast Simulation of Litz Wire Using Multilevel PEEC Method," *IEEE Transactions on Power Electronics*, vol. 35, no. 12, pp. 12 612–12 616, 2020.

[10] D. Kusiak, "The magnetic field and impedances in three-phase rectangular busbars with a finite length," *Energies*, vol. 12, no. 8, 2019. [Online]. Available: https://www.mdpi.com/1996-1073/12/8/1419

[11] A. Canova and L. Giaccone, "Numerical and Analytical Modeling of Busbar Systems," *IEEE Transactions on Power Delivery*, vol. 24, no. 3, pp. 1568–1578, 2009.

[12] P. Silvester, "The Accurate Calculation of Skin Effect in Conductors of Complicated Shape," *IEEE Transactions on Power Apparatus and Systems*, vol. PAS-87, no. 3, pp. 735–742, 1968.

[13] Z. Piatek, B. Baron, P. Jabłoński, T. Szczegielniak, D. Kusiak, and A. Pasierbek, "A numerical method for current density determination in three-phase bus-bars of rectangular cross section," *Przeglad Elektrotechniczny*, vol. 89, no. 8, pp. 294–298, 2013.

[14] A. Sancarlos-González, M. Pineda-Sanchez, R. Puche-Panadero, A. Sapena-Bano, M. Riera-Guasp, J. Martinez-Roman, J. Perez-Cruz, and J. Roger-Folch, "Application of the parametric proper generalized decomposition to the frequency-dependent calculation of the impedance of an ac line with rectangular conductors," *Open Physics*, vol. 15, no. 1, pp. 929–935, 2017. [Online]. Available: https://doi.org/10.1515/phys-2017-0113

[15] M. Matsuki and A. Matsushima, "EFFICIENT IMPEDANCE COMPUTATION FOR MULTICONDUCTOR TRANSMISSION LINES OF RECTANGULAR CROSS SECTION," *Progress In Electromagnetics Research B*, vol. 43, pp. 373–391, 2012.

[16] D. P. Labridis and P. S. Dokopoulos, "Electromagnetic forces in three-phase rigid busbars with rectangular cross-sections," *IEEE Transactions on Power Delivery*, vol. 11, no. 2, pp. 793–800, 1996.

[17] Joong Kyoung Kim, Sung Chin Hahn, Kyong Yop Park, Hong Kyu Kim, and Yeon Ho Oh, "Temperature rise prediction of EHV GIS bus bar by coupled magnetothermal finite element method," *IEEE Transactions on Magnetics*, vol. 41, no. 5, pp. 1636–1639, 2005.

[18] W. M. Frix and G. G. Karady, "A circuital approach to estimate the magnetic field reduction of nonferrous metal shields," *IEEE Transactions on Electromagnetic Compatibility*, vol. 39, no. 1, pp. 24–32, 1997.

[19] J.-R. Riba, "Analysis of formulas to calculate the ac resistance of different conductors' configurations," *Electric Power Systems Research*, vol. 127, pp. 93–100, 2015. [Online]. Available: https://www.sciencedirect.com/science/article/pii/S0378779615001649

[20] C. L. Holloway and E. F. Kuester, "DC Internal Inductance for a Conductor of Rectangular Cross Section," *IEEE Transactions on Electromagnetic Compatibility*, vol. 51, no. 2, pp. 338–344, 2009.

[21] M. Pineda-Sanchez, A. Sapena-Baño, J. Perez-Cruz, J. Martinez-Roman, R. Puche-Panadero, and M. Riera-Guasp, "Internal inductance of a conductor of rectangular cross-section using the proper generalized decomposition," *COMPEL - The international journal for computation and mathematics in electrical and electronic engineering*, vol. 35, no. 6, pp. 2007–2021, nov 2016.

[22] A. Hoshmeh and U. Schmidt, "A full frequency-dependent cable model for the calculation of fast transients," *Energies*, vol. 10, no. 8, 2017. [Online]. Available: https://www.mdpi.com/1996-1073/10/8/1158

[23] R. Escovar, S. Ortiz, and R. Suaya, "An improved long distance treatment for mutual inductance," *IEEE Transactions on Computer-Aided Design of Integrated Circuits and Systems*, vol. 24, no. 5, pp. 783–793, 2005.

[24] M. Shafieipour, Z. Chen, A. Menshov, J. De Silva, and V. Okhmatovski, "Efficiently computing the electrical parameters of cables with arbitrary cross-sections using the method-of-moments," *Electric Power Systems Research*, vol. 162, pp. 37–49, 2018. [Online]. Available: https://www.sciencedirect.com/science/article/pii/S0378779618301202

[25] D. N. Dyck and J. P. Webb, "Solenoidal current flows for filamentary conductors," *IEEE Transactions on Magnetics*, vol. 40, no. 2, pp. 810–813, 2004.

[26] S. Alfonzetti, G. Borzi, and N. Salerno, "A fast solving strategy for two-dimensional skin effect problems," *IEEE Transactions on Magnetics*, vol. 39, no. 3, pp. 1119–1122, 2003.

[27] D. De Zutter and L. Knockaert, "Skin effect modeling based on a differential surface admittance operator," *IEEE Transactions on Microwave Theory and Techniques*, vol. 53, no. 8, pp. 2526–2538, 2005.

[28] U. R. Patel, B. Gustavsen, and P. Triverio, "Proximity-Aware Calculation of Cable Series Impedance for Systems of Solid and Hollow Conductors," *IEEE Transactions on Power Delivery*, vol. 29, no. 5, pp. 2101–2109, 2014.

[29] T. Demeester and D. De Zutter, "Construction of the Dirichlet to Neumann Boundary Operator for Triangles and Applications in the Analysis of Polygonal Conductors," *IEEE Transactions on Microwave Theory and Techniques*, vol. 58, no. 1, pp. 116–127, 2010.

[30] U. R. Patel and P. Triverio, "Skin Effect Modeling in Conductors of Arbitrary Shape Through a Surface Admittance Operator and the Contour Integral Method," *IEEE Transactions on Microwave Theory and Techniques*, vol. 64, no. 9, pp. 2708–2717, 2016.

[31] P. de Arizon and H. W. Dommel, "Computation of Cable Impedances Based on Subdivision of Conductors," *IEEE Transactions on Power Delivery*, vol. 2, no. 1, pp. 21–27, 1987.

[32] R. A. Rivas and J. R. Marti, "Calculation of frequency-dependent parameters of power cables: matrix partitioning techniques," *IEEE Transactions on Power Delivery*, vol. 17, no. 4, pp. 1085–1092, 2002.

[33] M. P. Sánchez and L. S. Iribarnegary, "Magnetic Fields in Multiconductor Systems with Harmonic Currents," *Renewable energy & power quality journal*, vol. 1, pp. 614–619, 2003.

[34] K. Coperich, A. Ruehli, and A. Cangellaris, "Enhanced skin effect for partial-element equivalent-circuit (PEEC) models," *IEEE Transactions on Microwave Theory and Techniques*, vol. 48, no. 9, pp. 1435–1442, 2000.

[35] P. Silvester, "AC Resistance and Reactance of Isolated Rectangular Conductors," *IEEE Transactions on Power Apparatus and Systems*, vol. PAS-86, no. 6, pp. 770–774, 1967.

[36] ——, "Skin Effect in Multiple and Polyphase Conductors," *IEEE Transactions on Power Apparatus and Systems*, vol. PAS-88, no. 3, pp. 231–238, 1969.

[37] P. GRANEAU, "Alternating and Transient Conduction Currents in Straight Conductors of any Cross-section," *International Journal of Electronics*, vol. 19, no. 1, pp. 41–59, 1965. [Online]. Available: https://doi.org/10.1080/00207216508937798

[38] ——, "Computation of Losses and Inter-conductor Forces in Low-temperature A.C. Power Circuits," *International Journal of Electronics*, vol. 22, no. 1, pp. 1–18, 1967. [Online]. Available: https://doi.org/10.1080/00207216708937936

[39] W. T. Weeks, L. L. . Wu, M. F. McAllister, and A. Singh, "Resistive and inductive skin effect in rectangular conductors," *IBM Journal of Research and Development*, vol. 23, no. 6, pp. 652–660, 1979.

[40] C. L. Holloway, E. F. Kuester, A. E. Ruehli, and G. Antonini, "Partial and Internal Inductance: Two of Clayton R. Paul's Many Passions," *IEEE Transactions on Electromagnetic Compatibility*, vol. 55, no. 4, pp. 600–613, 2013.

[41] C. Ni, Z. Zhao, and X. Cui, "Quasi-Static Partial Inductance for Open and Closed Loops," *IEEE Transactions on Electromagnetic Compatibility*, pp. 1–7, 2021.

[42] H. J. Song, Y. Yoon, M. A. Steffka, J. Campbell, and R. W. Young, "A method for measuring partial inductance," in *2011 IEEE International Symposium on Electromagnetic Compatibility*, 2011, pp. 335–340.

[43] G. Antonini, A. Orlandi, and C. R. Paul, "Internal impedance of conductors of rectangular cross section," *IEEE Transactions on Microwave Theory and Techniques*, vol. 47, no. 7, pp. 979–985, 1999.

[44] C. Ni, Z. Zhao, and X. Cui, "Inductance Calculation Method Based on Induced Voltage," *IEEE Transactions on Magnetics*, vol. 53, no. 6, pp. 1–4, 2017.

[45] H. Hu, D. T. Blaauw, V. Zolotov, K. Gala, Min Zhao, R. Panda, and S. S. Sapatnekar, "Fast on-chip inductance simulation using a precorrected-FFT method," *IEEE Transactions on Computer-Aided Design of Integrated Circuits and Systems*, vol. 22, no. 1, pp. 49–66, 2003.

[46] E. Bleszynski, M. Bleszynski, and T. Jaroszewicz, "AIM: Adaptive integral method for solving large-scale electromagnetic scattering and radiation problems," *Radio Science*, vol. 31, no. 5, pp. 1225–1251, 1996.

[47] D. Freitas, M. Guerreiro das Neves, M. Almeida, and V. Maló Machado, "Evaluation of the longitudinal parameters of an overhead transmission line with non-homogeneous cross section," *Electric Power Systems Research*, vol. 119, pp. 478–484, 2015. [Online]. Available: https://www.sciencedirect.com/science/article/pii/S0378779614004027

[48] H. B. Dwight, "Geometric mean distances for rectangular conductors," *Electrical Engineering*, vol. 65, no. 8-9, pp. 536–538, 1946.

[49] Z. He, M. Celik, and L. Pileggi, "SPIE: Sparse Partial Inductance Extraction," in *Proceedings of the 34th Annual Design Automation Conference*, ser. DAC '97. New York, NY, USA: Association for Computing Machinery, 1997, p. 137–140. [Online]. Available: https://doi.org/10.1145/266021.266050

[50] D. C. Meeker, "Finite element method magnetics. ver. 4.2, apr. 21, 2009." [Online]. Available: https://www.femm.info/wiki/Download (accessed Aug. 27, 2021)

J. Martinez-Roman received his Ph.D. degree in Electrical Engineering from the Universitat Politècnica de València, Spain, in 2002. Currently he is Associate Professor with the Universitat Politècnica de València. His research interests are electrical machines and drives. He has participated in various international projects supported by the European Union. He has published several papers on electrical machines in international journals and conference proceedings.

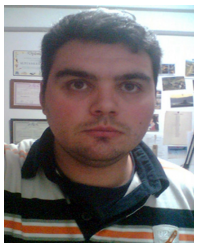

R. Puche-Panadero (M'09) received his M.Sc. degree in Automatic and Electronic Engineering in 2003, and his Ph.D. degree in Electrical Engineering in 2008, both from the Universitat Politècnica de València. He joined the Universitat Politècnica de València in 2006 and he is currently Associate Professor of Control of Electrical Machines. His research interests focus on induction motor diagnosis, numerical modelling of electrical machines, and advanced automation processes and electrical installations.

A. Sapena-Bano obtained its M.Sc. degree in 2009 and his Ph.D. degree in 2014 from the Universitat Politècnica de València (Spain), both in Electrical Engineering. Currently, he is Associate Professor with the Universitat Politècnica de València. His research interests focus on induction motor diagnostics, numerical modelling of electrical machines, and advanced automation processes and electrical installations.

J. Burriel-Valencia received his Ms.C. degree in Informatics Engineering in 2010, and his Ph.D. degree in Electrical Engineering in 2016, both from the Universitat Politècnica de València, Spain. Currently, he is Assistant Professor with the Department of Electrical Engineering of the Universitat Politècnica de València, and focuses his research on the development of expert systems for fault diagnosis.

C. Terron-Santiago obtained its M.Sc. degree in 2018 from the Universitat Politècnica de València (Spain), in Electrical Engineering. Currently, she is working as researcher with the Institute for Electrical Engineering, in the Universitat Politècnica de València. Her research interests focus on induction motor diagnostics, and numerical modelling of electrical machines.

M. Pineda-Sanchez (M'02) received the M.Sc. degree in industrial engineering and the Ph.D. degree in electrical engineering from the Universitat Politècnica de València, Valencia (Spain), in 1985 and 2004, respectively. Currently, he is full Professor with the Department of Electrical Engineering of the Universitat Politècnica de València. His research interests include electrical machines and drives, induction motor diagnosis and numerical simulation of electromagnetic devices.

M. Riera-Guasp (M'94-SM'12) received the M. Sc. degree in industrial engineering and the Ph.D. degree in electrical engineering from the Universitat Politècnica de València, Valencia (Spain), in 1981 and 1987, respectively. Currently, he is full Professor with the Department of Electrical Engineering, Universitat Politècnica de València. His research interests include condition monitoring of electrical machines, applications of signal analysis techniques to electrical engineering and efficiency in electric power applications.